

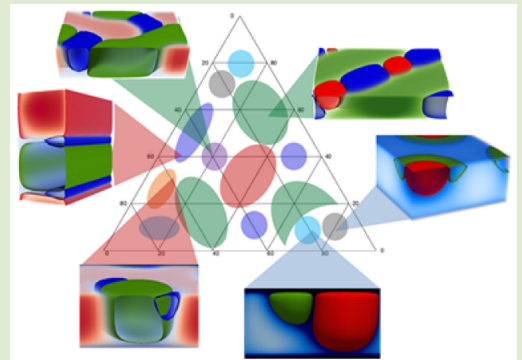
Phase Behavior of Ternary Polymer Brushes

Chester K. Simocko, Amalie L. Frischknecht, and Dale L. Huber*

Center for Integrated Nanotechnologies, Sandia National Laboratories, Albuquerque, New Mexico 87185, United States

Supporting Information

ABSTRACT: Ternary polymer brushes consisting of polystyrene, poly(methyl methacrylate), and poly(4-vinylpyridine) have been synthesized. These brushes laterally phase separate into several distinct phases and can be tailored by altering the relative polymer composition. Self-consistent field theory has been used to predict the phase diagram and model both the horizontal and vertical phase behavior of the polymer brushes. All phase behaviors observed experimentally correlate well with the theoretical model.



Polymer self-assembly can be used to create nanoscale features which can then be patterned using micron-scale photolithography.^{1–3} This patterning allows for high-throughput production on scales not easily achieved by traditional lithography.^{4–7} Polymer self-assembly is driven by mixing two or more immiscible polymers that are spatially constrained, such as block copolymers. In these systems macroscopic phase separation is not possible, so the polymers instead self-assemble into ordered nanoscale domains. This microphase separation, which minimizes the overall free energy of the system,^{8,9} is driven by the immiscibility of the polymers.

Patterned surfaces created by block copolymers have been thoroughly studied for use in biological, electronic, and membrane applications.^{10–12} As useful as block copolymers are, they have several significant drawbacks. First, the coatings are generally spin coated, meaning that only planar surfaces can be used. Also, sharp curves and right angles cause packing problems that require the addition of precise amounts of another component to relieve.³ Finally, in these systems the polymer is not attached to the substrate and is susceptible to removal by both chemical and mechanical means. Fortunately, block copolymers are not the only systems that undergo microphase separation. Polymer brushes are capable of forming stable coatings and have been studied on both planar surfaces and on nanoparticles¹³ for application in membranes, solid supports, and low friction surfaces.^{14–17} Microphase separation in binary polymer brushes is similar to that seen in block copolymer systems.^{18–21} Instead of the two immiscible polymer “blocks” being bound to each other, in a binary brush the polymers are spatially confined by being bound to the substrate. Our previous work used self-consistent field theory (SCFT) and surface-initiated free radical polymerization to systematically study the phase behavior in a polystyrene (PS)/poly(methyl methacrylate) (PMMA) binary brush. We were able to theoretically predict and then experimentally confirm

four distinct polymer phases, which in order of increasing mole fraction of PS were disordered, hemisphere, cylinder, and ripple phases.²²

Here we study the much richer phase behavior of ternary polymer brushes composed of PS, PMMA, and poly(4-vinylpyridine) (P4VP). SCFT and experiment agree that this system is able to create unique nanostructures not seen in block copolymer systems.

The phase behavior and morphologies of ternary brushes in the melt state were calculated using a field theoretic model introduced in our previous work.^{19,20} The polymers are modeled as continuous Gaussian chains tethered to the substrate, which is modeled as a hard, impenetrable wall. We assume that the free surface is neutral to all three polymers and that there is a large polymer–air surface tension, and so we also treat the free surface as a flat, hard wall. We consider monodisperse A, B, and C tethered homopolymers, with equal chain lengths N . Length scales in the simulation results are in units of R_g . Throughout this work, the ternary brush is assumed to have a height of $L_z = 3R_g$. Since the system is a melt, the height fixes the overall grafting density. Periodic boundary conditions are employed in the plane of the brush in the x and y directions. All calculations were started with random initial field configurations. Further details of the calculations can be found in the *Supporting Information*.

The interaction energies are modeled with Flory-type local contact interactions between A, B, and C polymer segments, denoted by the Flory parameters χ_{AB} , χ_{AC} , and χ_{BC} . The Flory–Huggins χ parameter for PS–PMMA is well-known and is about $\chi_{PS-PMMA} = 0.018$.²⁴ The other two χ parameters are

Received: November 6, 2015

Accepted: December 29, 2015

Published: January 7, 2016

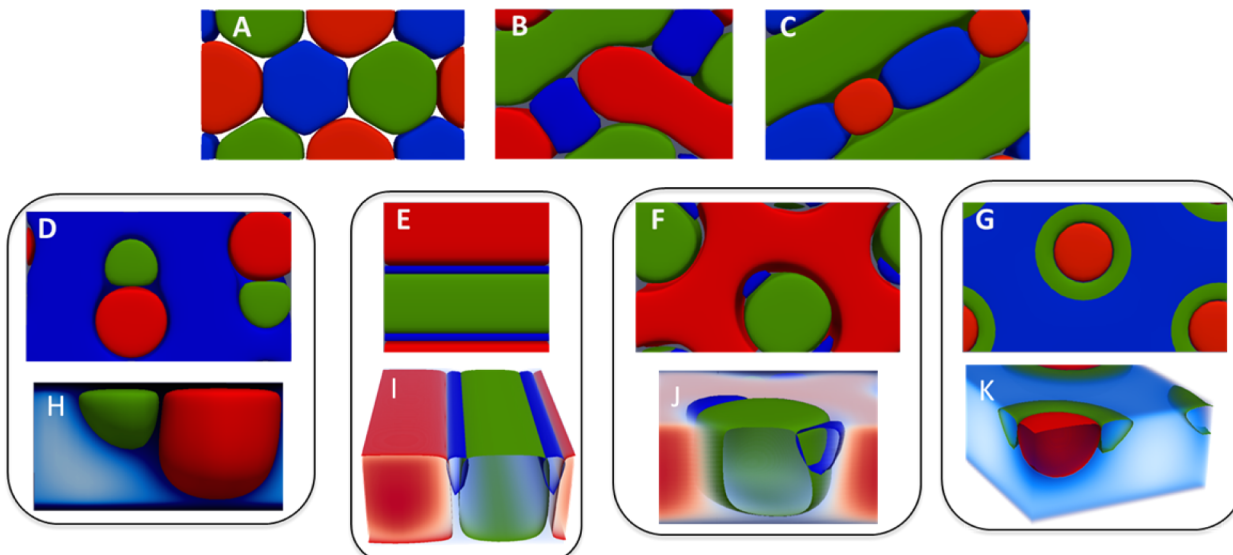


Figure 1. Equilibrium morphologies of ternary brush phases, shown by contour plots of polymers A (blue), B (green), and C (red): (A) checkerboard ($f_A = 0.333, f_B = 0.333, f_C = 0.334$); (B) basket ($f_A = 0.2, f_B = 0.4, f_C = 0.4$); (C) AC segmented ripple ($f_A = 0.3, f_B = 0.6, f_C = 0.1$); (D) BC lobed cylinder ($f_A = 0.7, f_B = 0.1, f_C = 0.2$); (E) A decorated ripple ($f_A = 0.1, f_B = 0.4, f_C = 0.5$; contour for A at $\phi_A = 0.25$); (F) decorated cylinder ($f_A = 0.1, f_B = 0.3, f_C = 0.6$); (G) ringed cylinder ($f_A = 0.8, f_B = 0.1, f_C = 0.1$; contour for B at $\phi_B = 0.15$). (H, I, J, K) Vertical slices of D, E, F, and G.

considerably larger, $\chi_{\text{PMMA-P4VP}} \approx 0.065$ and $\chi_{\text{PS-P4VP}} \approx 0.32$ – 0.347 .^{25,26} For the experimental molecular weights of around 100 kDa, we have a degree of polymerization $N \approx 1000$ and thus χN values of about $\chi_{\text{PS-PMMA}}N \approx 18$, $\chi_{\text{PMMA-P4VP}}N \approx 65$, and $\chi_{\text{PS-P4VP}}N \approx 320$, with the latter two in the strong segregation regime. As found previously, it is increasingly difficult to obtain converged SCFT solutions at large χN , but based on previous experience with binary brushes and block copolymers, we also expect the boundaries between the different microphase-separated states to be relatively insensitive to χN at large χN .²³ We therefore chose to calculate a representative phase diagram with asymmetric values of the interaction parameters to mimic the experimental system, with $\chi_{AB}N = 10$, $\chi_{AC}N = 12$, and $\chi_{BC}N = 16$. We will identify A = PMMA, B = PS, and C = P4VP.

Figure 2 shows the SCFT ternary phase diagram, calculated for all volume fractions f_A , f_B , and f_C of the three polymers in increments of 0.1. The additional point in the middle of the diagram is for $f_A = f_B = 0.333$ and $f_C = 0.334$. The reported phase is the one with the lowest free energy; in some cases a different phase has only a slightly higher free energy. We find seven different phase morphologies as shown in Figure 1. The images in Figure 1A–G are contour plots of the top surface of the brush, showing where each species' volume fraction profile $\phi_a(\mathbf{r}) = 0.5$ unless otherwise noted.

The mean-field phase diagram for the ternary melt brush is built on motifs found previously in the binary melt brush phase diagram, namely, the ripple, cylinder, and hemisphere phases. At near equal volume fractions of all three polymers, we find the checkerboard phase shown in Figure 1A, where each polymer forms a compact, cylindrical domain and the overall phase has hexagonal symmetry. This phase is slightly lower in free energy than a three-color ripple phase consisting of stripes of A, B, and C phases. The basket phase of Figure 1B was only found to have the lowest free energy at $f_A = 0.2, f_B = 0.2$, and $f_C = 0.4$, where it has a lower free energy density than the checkerboard phase by $0.0032kT/R_g^3$. The segmented ripple

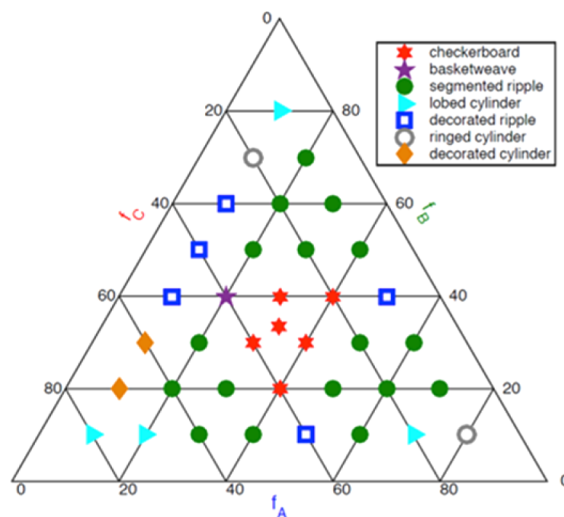


Figure 2. Mean-field phase diagram.

phases consist of a ripple of one polymer, separated by a ripple structure consisting of alternating domains of the other two polymers. These phases occur at moderately asymmetric compositions, typically when one of the components has a volume fraction of 0.5–0.6, and basically consist of combinations of the ripple and cylinder phases from the binary brush phase diagram (Figure 1C). When at least one of the polymer components has a volume fraction of 0.1, we find a larger variety of phases. In all of these cases, the minority domains with $f = 0.1$ form “hemisphere” morphologies, where the domain does not extend through the entire thickness of the brush but is instead located near the top surface (Figures 1H to 1J). This is again consistent with the binary brush phase diagram, in which we find a transition from cylinders to hemispheres at about $f = 0.13$.²³

The lobed cylinder phases consist of hexagonally packed domains of two phase-separated domains, dispersed in a matrix

of the third polymer (Figure 1D). The decorated ripple phases consist of a ripple phase of two of the polymers, “decorated” by a small amount of the third minority polymer, as shown in Figure 1E.²⁷ Finally, in both the decorated and ringed cylinder phases, there are hexagonally packed cylindrical domains of one polymer in a matrix of another; the third polymer “decorates” the cylindrical domain either by having small domains on each side (decorated cylinder, Figure 1F) or by surrounding it in a ring (ringed cylinder, Figure 1G).

Figures 1H, I, J, and K consist of vertical slices of the contour plots from Figures 1D, E, F, and G, respectively. Figures 1H and 1J correspond to Figures 1D and 1F, lobed cylinders, and decorated cylinders, which demonstrate that the larger minority domain forms full cylinders while the smallest domain forms only hemispheres. Figures 1E and 1I show that in the decorated ripple phase two of the domains (here B and C) extend through the brush, but the third domain (A) is a ripple that only forms at the surface of the brush. Figure 1G and K, the ringed cylinder, consists of a central cylinder surrounded by a minority toroid-like domain around the cylinder.

The free energy per unit volume of the various phases ranges from a minimum of $5.39958kT/R_g^3$ (at $f_A = 0.8, f_B = 0.1$) to a maximum of $6.81697kT/R_g^3$ (at $f_A = 0.3, f_B = 0.3$). In general, the free energy is higher for phases with significant volume fractions of all three polymers since these phases have more high energy interfaces than phases with less interface. Thus, the highest free energy phases are the checkerboard and basket phases, while the lowest free energy phases are the lobed and ringed cylinder phases (see also Figure SI3 in the SI).

To test these results experimentally, ternary polymer brushes were synthesized by sequentially polymerizing PS, PMMA, and P4VP from a silicon wafer. The samples were solvent vapor and thermally annealed and then were analyzed via ellipsometry, gel permeation chromatography (GPC), and atomic force microscopy (AFM). Further experimental details are given in the Supporting Information. Table SI2 shows the characterization of the polymer brushes. The molecular weights were obtained from the polymers in free solution, which are assumed to have the same molecular weight as the bound polymer in surface bound free radical polymerizations.^{28,29} In all cases, Table SI1 shows that R_g is significantly greater than the average distance between grafting points l , demonstrating that the polymer brushes are in the extended brush regime. The samples listed in Table SI2 correspond to the AFM phase images in Figures 3 and 4.

Figure 3 demonstrates that there is strong horizontal phase separation between the polymers in the ternary brushes, as is evident in the variety of observed microstructures. The domains in the AFM images are assigned colors based on the observed AFM phase information, with the appropriate polymer for each domain determined by the known polymer volume fraction in each sample. An example of how the polymer domains are determined from the original AFM phase images is given in the Supporting Information for sample 4B. The phase behavior of the brushes can be tailored by changing the polymer fractions of PS (green), PMMA (blue), and P4VP (red). Figure 3A is consistent with a decorated cylinder phase. Figure 3B is consistent with a segmented/decorated ripple phase with short PS-rich areas surrounded by a PMMA ripple. Figures 3C and D are both indicative of decorated or lobed cylinder phases.

In Figure 4 we compare the results from large cell SCFT simulations with corresponding AFM images of the experimental brushes at similar polymer volume fractions. The

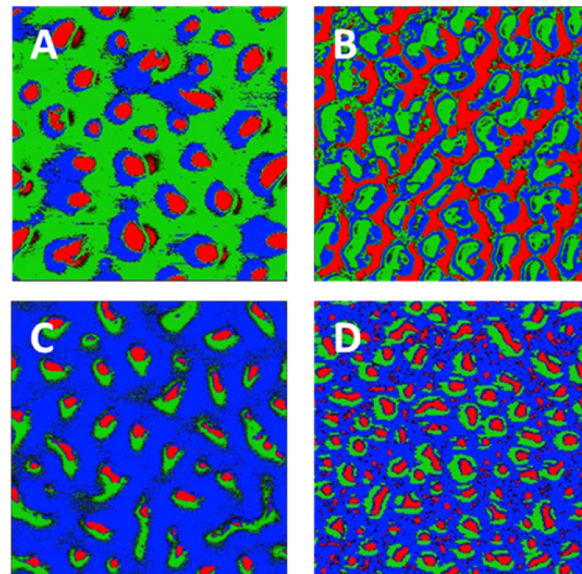


Figure 3. AFM phase images of ternary polymer brushes following thermal annealing. The polymer fractions are (A) $f_{\text{PMMA}} = 0.26, f_{\text{PS}} = 0.50, f_{\text{P4VP}} = 0.24$, (B) $f_{\text{PMMA}} = 0.38, f_{\text{PS}} = 0.21, f_{\text{P4VP}} = 0.41$, (C) $f_{\text{PMMA}} = 0.49, f_{\text{PS}} = 0.24, f_{\text{P4VP}} = 0.27$, and (D) $f_{\text{PMMA}} = 0.50, f_{\text{PS}} = 0.37, f_{\text{P4VP}} = 0.13$. Each image is $1 \mu\text{m} \times 1 \mu\text{m}$.

experimental images have lateral dimensions of $1 \mu\text{m} \times 1 \mu\text{m}$, while each SCFT figure is $50R_g$ on a side. Since typical R_g values for the experimental polymers are about 9 nm (see Table SI2), the experimental figures are roughly twice the size of the SCFT figures. The simulations were started from a random field configuration and were quenched immediately to the final χN values, and so they include defects. These defects are also present in the experimental systems and make comparisons with the SCFT more realistic than with the ideal, unit-cell morphologies of Figure 1.

Comparing the large cell SCFT simulations with the AFM phase images yields many similarities. In particular, these four systems show good agreement between the predicted and observed phase at nearly the same polymer volume fractions. Figure 4A is consistent with an A (PMMA) decorated ripple phase. Figure 4B is consistent with an AB (PMMA–PS) decorated or ringed cylinder phase. Simulation 4C corresponds well to the AFM image, with both simulation and experiment in the basket weave phase. Finally, both the experiment and simulation in 4D consist of nearly equal fractions of each polymer and fall into the checkerboard regime. The difference in details of the morphology seen in Figure 4D is a result of the difficulty in thresholding the image to display three domains. It is also possible that since there is no continuous domain in this phase there is some vertical phase separation of the brushes in the experimental system.

The experimental brushes are more disordered than the large cell SCFT simulations. One cause of this disorder is fluctuations in the location of grafting points in the experiments. We previously showed that inhomogeneities in the grafting density lead to increased disorder in large cell SCFT simulations of binary brushes and closer agreement with experiment;^{22,30} this will be further explored in future work on ternary brushes.

Experimentally, the decorated and/or ringed cylinder phases (Figures 3A, 3C, 3D and Figure 4B) appear over a wider range of volume fractions than in the SCFT phase diagram. This

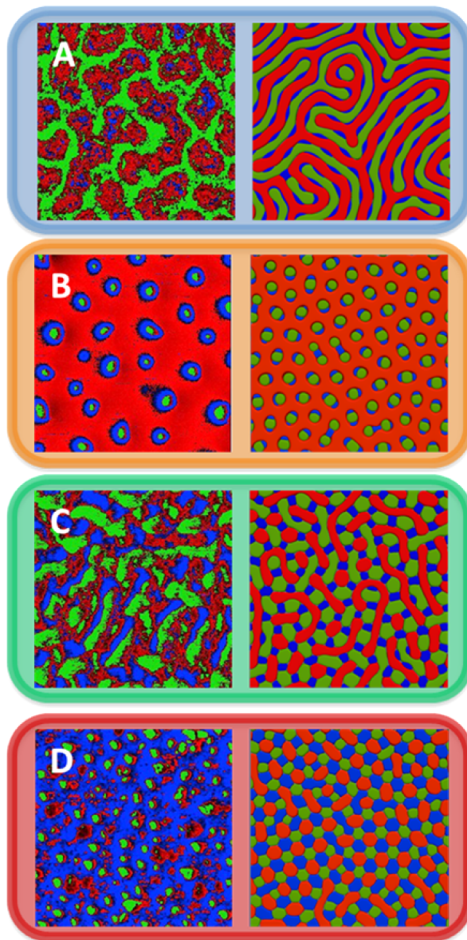


Figure 4. Comparing experimental AFM images of ternary brushes with large-scale SCFT simulations: (A) $f_{\text{PMMA}} = 0.08, f_{\text{PS}} = 0.42, f_{\text{P4VP}} = 0.50; f_A = 0.1, f_B = 0.4, f_C = 0.5$ (contour for A at $\phi_A = 0.25$), (B) $f_{\text{PMMA}} = 0.18, f_{\text{PS}} = 0.18, f_{\text{P4VP}} = 0.64; f_A = 0.1, f_B = 0.2, f_C = 0.7$; (C) $f_{\text{PMMA}} = 0.21, f_{\text{PS}} = 0.46, f_{\text{P4VP}} = 0.33; f_A = 0.2, f_B = 0.4, f_C = 0.4$, (D) $f_{\text{PMMA}} = 0.35, f_{\text{PS}} = 0.28, f_{\text{P4VP}} = 0.37; f_A = 0.35, f_B = 0.27, f_C = 0.38$.

could easily be due to differences in χ parameters. In particular, experimentally $\chi_{\text{PS-P4VP}}$ is much larger than both $\chi_{\text{PS-PMMA}}$ and $\chi_{\text{PMMA-P4VP}}$, with ratios among the three parameters being about 17.8:3.6:1, compared with the values of 1.33:1.2:1 used in the SCFT calculations. Additional SCFT unit cell calculations with $\chi_{AB}N = \chi_{AC}N = 10$ and $\chi_{BC}N = 16$ (to investigate a wider difference between $\chi_{BC}N$ and the other two χN 's) show that the ringed cylinder phase expands to include more areas near each corner of the phase diagram, including to $f_A = 0.1$ and $f_B = 0.2$, closer to the composition of Sample 4B. Thus, we expect the phases to shift their locations in the phase diagram somewhat depending on the details of the χ parameters and in particular their relative values.

Figure 5 ties together the results from the SCFT simulations and the experimental results onto one phase diagram. The phases are approximately denoted by different colors and are extrapolated from the SCFT simulations. The phases of the experimental brushes as determined visually from Figures 3 and 4 are placed on the phase diagram. While there is general agreement between experimental and theoretical results, with the same phases appearing in the same general area of the phase diagram, there are some differences in the precise locations, specifically the experimental samples from Figure 3. These

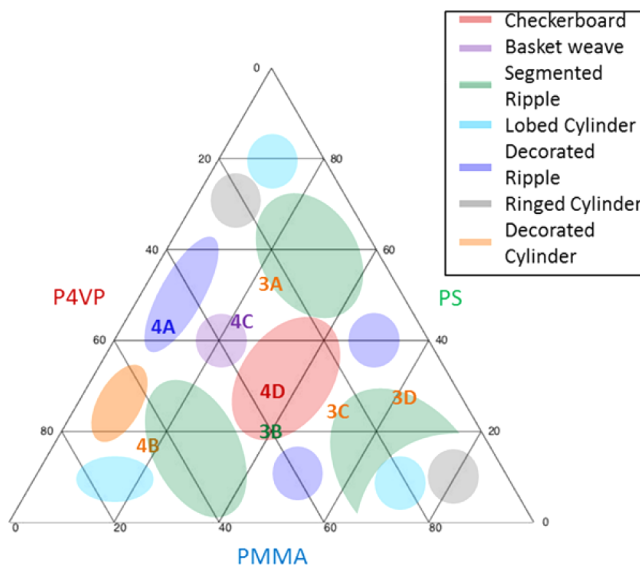


Figure 5. Phase diagram with approximate phase regions (shaded areas) determined via SCFT. Experimental results for each sample are shown by AFM figure number and colored by the experimental phase (3A, 3C, 3D, 4B: decorated cylinder; 3B: segmented ripple; 4A: decorated ripple; 4C, basket weave; 4D, checkerboard).

samples all fall on the edge of known phase areas; in these areas the phase behavior is only approximate. There are two likely explanations for these discrepancies in the location of the borders between phases. One is that the phases are similar in energy, so experiments are prone to getting kinetically trapped in local energy minima and may not reflect thermodynamic ground states. The other potential source for disagreement is that the χN values for the experimental systems are much higher than the modeled values, and while the models are not particularly sensitive to χN at high values, it could lead to inaccuracies in the precise locations of phase boundaries. Additional sources of discrepancy are that the degrees of polymerization are not equal among all the polymers, and the experimental brushes are not perfectly uniform in height (see Table S12). Even though the precise locations on the phase diagram disagree, all phases seen experimentally are also seen using SCFT. Overall we find remarkably good agreement in phase behavior between experiment and a simplified theory for such a complicated system.

In conclusion, we have synthesized ternary polymer brushes consisting of PS, PMMA, and P4VP, and these brushes have been shown to exist as extended brushes. We have demonstrated that ternary polymer brushes exhibit a rich phase behavior that consists of a range of horizontally phase-separated patterns. This behavior has been modeled using SFCT, and seven distinct phase regimes have been identified. Moreover, the simulations correlate strongly with experimental results, displaying similar phase behavior for similar polymer volume fractions.

While some of the patterns are familiar in appearance to other self-assembled structures, others are unique and represent useful new patterns for nanotechnology. In particular, four of the phases identified can exist with one or more of the features pinned to the surface but distant from the substrate. These types of structures could template materials with interesting optical and electronic interactions with a substrate material.

■ ASSOCIATED CONTENT

§ Supporting Information

The Supporting Information is available free of charge on the ACS Publications website at DOI: [10.1021/acsmacrolett.5b00792](https://doi.org/10.1021/acsmacrolett.5b00792).

Detailed experimental procedures and simulation methods ([PDF](#))

■ AUTHOR INFORMATION

Corresponding Author

*E-mail: dale.huber@sandia.gov.

Author Contributions

The manuscript was written through contributions of all authors.

Notes

The authors declare no competing financial interest.

■ ACKNOWLEDGMENTS

This work was supported by the U.S. Department of Energy, Office of Science, Basic Energy Sciences, Materials Sciences and Engineering Division. Ellipsometry and Atomic Force Microscopy were performed at the Center for Integrated Nanotechnologies, an Office of Science User Facility operated for the U.S. Department of Energy (DOE) Office of Science. Sandia National Laboratories is a multiprogram laboratory managed and operated by Sandia Corporation, a wholly owned subsidiary of Lockheed Martin Corporation, for the U.S. Department of Energy's National Nuclear Security Administration under contract DE-AC04-94AL85000.

■ REFERENCES

- (1) Albert, J. N. L.; Epps, T. H. *Mater. Today* **2010**, *13* (6), 24–33.
- (2) Kim, S. O.; Solak, H. H.; Stoykovich, M. P.; Ferrier, N. J.; De Pablo, J. J.; Nealey, P. F. *Nature* **2003**, *424* (6947), 411–414.
- (3) Stoykovich, M. P.; Müller, M.; Kim, S. O.; Solak, H. H.; Edwards, E. W.; de Pablo, J. J.; Nealey, P. F. *Science* **2005**, *308*, 1442–1446.
- (4) Hamley, I. W. *Angew. Chem., Int. Ed.* **2003**, *42*, 1692–1712.
- (5) Park, M.; Harrison, C.; Chaikin, P. M.; Register, R. A.; Adamson, D. H. *Science* **1997**, *276*, 1401–1404.
- (6) Tang, C.; Lennon, E. M.; Fredrickson, G. H.; Kramer, E. J.; Hawker, C. J. *Science* **2008**, *322*, 429–432.
- (7) Durand, W. J.; Blachut, G.; Maher, M. J.; Sirard, S.; Tein, S.; Carlson, M. C.; Asano, Y.; Zhou, S. X.; Lane, A. P.; Bates, C. M.; Ellison, C. J.; Willson, C. G. *J. Polym. Sci., Part A: Polym. Chem.* **2015**, *53* (2), 344–352.
- (8) Bates, F. S.; Fredrickson, G. H. *Phys. Today* **1999**, *52* (2), 32–38.
- (9) Fasolka, M. J.; Mayes, A. M. *Annu. Rev. Mater. Res.* **2001**, *31*, 323–355.
- (10) Aizawa, M.; Buriak, J. *Chem. Mater.* **2007**, *19*, 5090–5101.
- (11) Gao, H. M.; Liu, H.; Lu, Z.-Y.; Sun, Z.-Y.; An, L.-J. *J. Chem. Phys.* **2013**, *138* (22), 224905.
- (12) Li, L.; Chen, C.; Li, J.; Zhang, A.; Liu, X.; Xu, B.; Gao, S.; Jin, G.; Ma, Z. *J. Mater. Chem.* **2009**, *19* (18), 2789.
- (13) Tang, S.; Fox, T. L.; Lo, T.-Y.; Horton, J. M.; Ho, R.-M.; Zhao, B.; Stewart, P. L.; Zhu, L. *Soft Matter* **2015**, *11* (27), 5501–5512.
- (14) Luzinov, I.; Minko, S.; Tsukruk, V. V. *Prog. Polym. Sci.* **2004**, *29* (7), 635–698.
- (15) Barbey, R.; Lavanant, L.; Paripovic, D.; Schuwer, N.; Sugnaux, C.; Tugulu, S.; Klok, H. *Chem. Rev.* **2009**, *109*, 5437–5527.
- (16) Zhao, B.; Brittain, W. J. *Prog. Polym. Sci.* **2000**, *25*, 677–710.
- (17) Price, A. D.; Huber, D. L. *Polym. Chem.* **2013**, *4* (5), 1565.
- (18) Lemieux, M.; Usov, D.; Minko, S.; Stamm, M.; Shulha, H.; Tsukruk, V. V. *Macromolecules* **2003**, *36* (19), 7244–7255.
- (19) Wang, J.; Müller, M. *J. Phys. Chem. B* **2009**, *113* (33), 11384–11402.
- (20) Marko, J. F.; Witten, T. A. *Phys. Rev. Lett.* **1991**, *66* (11), 1541–1544.
- (21) Calabrese, D. R.; Ditter, D.; Liedel, C.; Blumfield, A.; Zentel, R.; Ober, C. K. *ACS Macro Lett.* **2015**, *4*, 606–610.
- (22) Price, A. D.; Hur, S.-M.; Fredrickson, G. H.; Frischknecht, A. L.; Huber, D. L. *Macromolecules* **2012**, *45* (1), 510–524.
- (23) Hur, S.-M.; Frischknecht, A. L.; Huber, D. L.; Fredrickson, G. H. *Soft Matter* **2011**, *7* (19), 8776.
- (24) Eitouni, H. B.; Balsara, N. P. *Physical Properties of Polymer Handbook*; Springer, 2007.
- (25) Han, S. H.; Kon Kim, J. *React. Funct. Polym.* **2009**, *69* (7), 493–497.
- (26) Zha, W.; Han, C. D.; Lee, D. H.; Han, S. H.; Kim, J. K.; Kang, J. H.; Park, C. *Macromolecules* **2007**, *40*, 2109–2119.
- (27) The B and C decorated ripple phases have discontinuous domains of B and C, respectively, decorating the ripples, unlike the continuous A domain in [Figure 1E](#). See [Figure SI2](#).
- (28) Boven, G.; Oosterling, M. L. C. M.; Challa, G.; Jan, A. *Polymer* **1990**, *31*, 2377–2383.
- (29) Minko, S.; Sidorenko, A.; Stamm, M.; Gafijchuk, G.; Senkovsky, V.; Voronov, S. *Macromolecules* **1999**, *32*, 4532–4538.
- (30) Hur, S. M.; Frischknecht, A. L.; Huber, D. L.; Fredrickson, G. H. *Soft Matter* **2013**, *9* (22), 5341.